

Bell inequalities as a tool to probe quantum chaos

Albert Aloy,^{1,2,*} Guillem Müller-Rigat,³ Maciej Lewenstein,^{3,4} Jordi Tura,^{5,6} and Matteo Fadel^{7,†}

¹*Institute for Quantum Optics and Quantum Information,
Austrian Academy of Sciences, Boltzmannngasse 3, A-1090 Vienna, Austria*

²*Vienna Center for Quantum Science and Technology (VCQ),
Faculty of Physics, University of Vienna, Vienna, Austria*

³*ICFO-Institut de Ciències Fòniques, The Barcelona Institute of Science and Technology, Castelldefels (Barcelona) 08860, Spain.*

⁴*ICREA, Pg. Lluís Companys 23, 08010 Barcelona, Spain.*

⁵*(aQa^L) Applied Quantum Algorithms, Universiteit Leiden*

⁶*Instituut-Lorentz, Universiteit Leiden, P.O. Box 9506, 2300 RA Leiden, The Netherlands*

⁷*Department of Physics, ETH Zürich, 8093 Zürich, Switzerland*

We introduce a permutationally invariant multipartite Bell inequality for many-body three-level systems and use it to explore a possible connection between the presence of nonlocality and quantum chaos. For this, we interpret the Bell operator resulting from fixing the measurement settings as a system Hamiltonian and explore the energy level spacing distribution for different measurement choices and SU(3) irreducible representations. Interestingly, we find that in every irreducible representation displaying nonlocality, the measurement settings yielding maximal violation result in a Bell operator whose energy level spacing distribution signals the absence of quantum chaos. This situation changes when the measurement settings slightly depart from the optimal ones, as we generally observe a level spacing distribution characteristic of chaotic systems. Our work suggests an intriguing connection between Bell nonlocality, quantum chaos and random matrix theory. These subjects belonged to the beloved areas of the late Fritz Haake, and we dedicate this paper to his memory.

Nonlocality is a quantum resource that enables tasks impossible by classical means, a main example being the violation of Bell inequalities [1]. Considerable theoretical and experimental progress has been recently made in the detection and characterization of nonlocality, also in many-body scenarios. However, the implications of nonlocal correlations in relation to macroscopic physical properties and observables of multipartite systems remain unclear.

For systems composed of many spin-1/2 particles, several methods and inequalities have been derived for detecting nonlocality and Bell correlations in a practical and scalable way [2]. This made possible to unveil interesting connections between the onset of nonlocality and phase transitions [3], quantum-critical points [4], and metrological advantage [5]. On the other hand, Bell inequalities for many multi-level systems (such as spin- S with $S \geq 1$) have been studied in only a few works [6, 7]. In this case, it is natural to consider Bell scenarios with $m \geq 2$ inputs and $d \geq 3$ (typically $d = 2S + 1$) outputs per party. Notoriously, the discovery of useful inequalities in such scenarios becomes extremely hard as m and d increase, because enumerating all tight inequalities scales as $\mathcal{O}((d^{mn})^{\lfloor D/2 \rfloor})$, where $D \in \mathcal{O}((dm)^n)$ and n is the number of parties [8].

To mitigate such a prohibitive scaling, a successful approach to facilitate nonlocality detection in the large n regime relies on focusing on few-body correlations only, as well as on exploiting symmetries already present in physical systems of interest. Examples include Bell inequalities involving one- and two-body observables with translational [9, 10] and permutational invariance [11–15], which can make the complexity of the Bell scenario scale polynomially in n . This enabled the experimental detection of Bell correlations in ensembles of $n \approx 500$ [16] and $n \approx 5 \cdot 10^5$ [17] spin-1/2 particles. To date, however, no experiment reported the detection of Bell

correlations in ensembles of particles with larger spin.

Systems of spin-1 or, more generally, of three-level particles play an important role in nuclear shell models [18–20], ultracold atomic ensembles [21–24] and in solid-state physics [25–27]. This motivated the development of ideas to simulate qudit Hamiltonians using trapped ions, superconducting circuits and ultracold atoms. Moreover, it was noted that such SU(3) models provide a minimal example of autonomous chaotic dynamics, as opposed to SU(2) models where quantum chaos is typically observed by inducing time-dependent interactions or periodic driving [28, 29].

While classical chaos is associated to an exponentially fast growing distance between phase-space trajectories, quantum chaos is often associated to spectral properties of the system’s Hamiltonian. The celebrated Bohigas-Giannoni-Schmit (BGS) conjecture [30] suggests that the spectrum statistics of quantum systems whose classical limit show chaotic behaviour are expected to be characterized by correlated energy levels similar to the ones encountered in Random Matrix Theory [31, 32]. A Poisson distribution of energy-level spacing is a characteristic indicator of a system that is integrable in the classical limit, while a Wigner-Dyson distribution of energy-level spacing is an indicator of chaotic dynamics [32].

In this work, we investigate the connection between quantum chaos and the presence of nonlocality. To this end, we introduce a three-outcome permutationally invariant Bell inequality (PIBI) from which we derive a Bell operator for multipartite three-level systems. We show that, depending on the chosen SU(3) representation, the Bell operator shows energy level spacing distributions characteristic of an integrable (resp. chaotic) model and generically the presence (resp. absence) of nonlocality. Our work sheds light on a possible connection between quantum correlations, the dynamical properties of a quantum system and random matrix theory.

A three-level PIBI and its corresponding Bell operator.–

For our analysis we introduce the multipartite two-setting three-outcome PIBI

$$B = (\mathcal{P}_{0|0} + \mathcal{P}_{0|1} + \mathcal{P}_{1|0} + \mathcal{P}_{1|1}) + \quad (1)$$

$$(\mathcal{P}_{00|00} + \mathcal{P}_{00|11} + \mathcal{P}_{11|00} + \mathcal{P}_{11|11}) - 2(\mathcal{P}_{01|01} + \mathcal{P}_{01|10}) \geq 0,$$

where $\mathcal{P}_{a|x} = \sum_{i \in [n]} p_i(a|x)$ represents the collective one-body conditional probability of obtaining outcome a for measurement setting x . Analogously, $\mathcal{P}_{ab|xy} = \sum_{i \neq j \in [n]} p_{ij}(ab|xy)$ represents the collective two-body conditional probability. In the Supplementary Material [33] we prove that Eq. (1) is indeed a Bell Inequality by showing that it has classical bound $\beta_c = 0$. Therefore, observing $B < 0$ signals nonlocal correlations.

To show that Bell inequality (1) can be violated by quantum mechanics, one has to find appropriate quantum states and measurements. To this end, we associate each measurement setting to a self-adjoint operator, such that Eq. (1) can be written as a Bell operator $\mathcal{B}(\theta)$, where θ is a vector parametrizing a specific measurement setting. The maximum quantum violation of the inequality can then be related to $\min_{\theta} \lambda_{\min}(\mathcal{B}(\theta))$, where λ_{\min} indicates the minimum eigenvalue. To carry out this minimization over θ for qutrits, we need a way to parametrize measurements. Contrary to the two-level case, *i.e.* $SU(2)$, where any local measurement can be efficiently parametrized by two angles, for higher-dimensional systems the parametrization is somewhat more involved [34].

For this work, we adopt the following continuous parametrization of unitary $SU(3)$ operators. We start by choosing a set of unitaries $\{U_0, \dots, U_{m-1}\}$, all with the same spectrum ordered by complex phase argument based on d -roots of unity $\{1, \zeta, \dots, \zeta^{d-1}\}$, where $\zeta = e^{i2\pi/d}$. Taking $d = 3$, we consider the Heisenberg-Weyl operators X and Z , which act on the computational basis as $X|\alpha\rangle = |\alpha + 1 \pmod{d}\rangle$ and $Z|\alpha\rangle = \zeta^\alpha |\alpha\rangle$ [35]. These satisfy $X^d = Z^d = \mathbb{I}$. In order to parameterize any unitary of $SU(3)$, we take a set of generators g_ℓ such that $V_\ell = e^{ig_\ell}$ are the elements of the set $\{X, Z, X^2, XZ, ZX, XZ^2, X^2Z, Z^2X, X^2Z^2\}$. Note that this choice is sufficient for g_ℓ to generate the Lie algebra $\mathfrak{su}(3)$.

For simplicity, here we consider that the measurement outcomes are ζ^i , as a generalization of the ± 1 outcomes one typically associates with the $d = 2$ case with Pauli matrices. Therefore, we are going to parameterize measurement operators as unitaries with spectrum ζ^i . Note that the fact that these are non-Hermitian is irrelevant, as the only relevant information needed is the basis in which these unitaries diagonalize [36]. Such basis will then be used to create the rank-1 projectors used to construct \mathcal{B} . To this end, let us define

$$g(\theta) := g_0 + \sum_{\ell=1}^M \theta_\ell (g_\ell - g_0), \quad (2)$$

where $\theta \in \mathbb{R}^M$, so that we have the desired unitary parametrization

$$U(\theta) := e^{ig(\theta)} D e^{-ig(\theta)}, \quad (3)$$

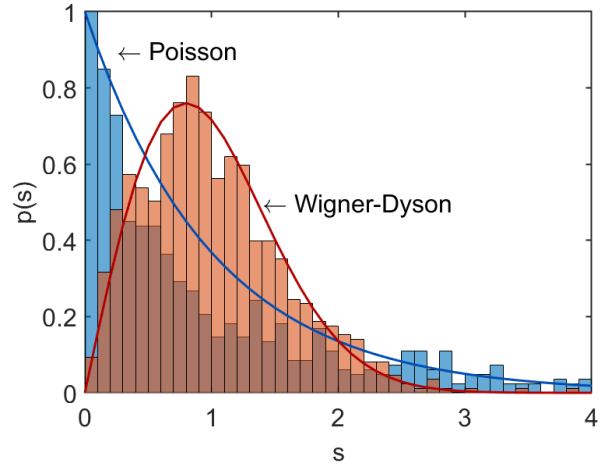


FIG. 1. Nearest-neighbour spacing distributions (NNSD) for PIBI (1) with $n = 25$ and optimal measurement settings. The irreps $(p, q) = (21, 2)$ (in blue) and $(9, 8)$ (in red) have been chosen for illustrative purposes, which in the symmetric subspace have 825 and 855 eigenvalues, respectively. Solid lines are fits using the Brody distribution Eq. (5), which interpolates between Poisson ($\omega \sim 0$, typical of an integrable system) and Wigner-Dyson distributions ($\omega \sim 1$, typical of a chaotic system).

where D is a diagonal matrix containing eigenvalues ζ^i . Concluding, instead of directly combining different unitaries U to obtain new ones, we have moved the parametrization to the Hermitian matrices g_ℓ which form a \mathbb{R} -vector space. Therefore, by varying g_ℓ using the parametrization in Eq. (2) we have obtained an interpolating function $U(\theta)$ in Eq. (3), which allows us to implement typical numerical see-saw and gradient descend optimization techniques.

For each measurement setting θ , via the inverse Fourier transform, we obtain the corresponding projectors $P_{j,k} = (\zeta^{0 \cdot j} U_k^3 + \zeta^{1 \cdot j} U_k^2 + \zeta^{2 \cdot j} U_k)/3$, where $j \in \{0, 1, 2\}$ labels the measurement outcomes and $k \in \{0, 1\}$ the measurement settings. In principle, the two measurement settings $\theta_k^{(i)}$ can be chosen differently for every party $i \in \{1, \dots, n\}$, but this would result in a too demanding optimization task. Therefore, we restrict ourselves to the same two measurement settings for every party, *i.e.* $\theta_k^{(i)} = \theta_k$, as numerical evidence supports the intuition that this choice is sufficient for permutationally invariant Bell inequalities [37].

By virtue of Schur-Weyl duality, PI Bell operators block-diagonalize in a symmetry-adapted basis in blocks of polynomial size [3]. These are indexed by the irreducible representations of the permutation group. Therefore, we can further restrict our search for the optimal measurements to each different blocks separately. We outline the details of this restricted optimization in the supplementary material [33].

SU(3) and quantum chaos.– The Hilbert space of a three-level particle is spanned by the basis vectors $|0\rangle = (1, 0, 0)^T$, $|1\rangle = (0, 1, 0)^T$ and $|2\rangle = (0, 0, 1)^T$. The transition from state $|\beta\rangle$ to $|\alpha\rangle$ is then described by one of the nine ladder operators

$\tau_{\alpha\beta} = |\alpha\rangle\langle\beta|$, for $\alpha, \beta \in \{0, 1, 2\}$. For a system of n three-level particles we introduce the collective operators $S_{\alpha\beta} = \sum_i \tau_{\alpha\beta}^{(i)}$, where $\tau_{\alpha\beta}^{(i)}$ denotes the operator $\tau_{\alpha\beta}$ applied on the i th particle. Note that we have $S_{00} + S_{11} + S_{22} = n\mathbb{I}$. Following the convention used in particle physics, we define the third component of the isospin $T_3 = (S_{00} - S_{11})/2$ and the hypercharge $Y = (S_{00} + S_{11} - 2S_{22})/2$. An irreducible representation of $SU(3)$ (*irrep* for short) is uniquely characterized by its highest-weight vector $|\mu\rangle$, which is defined as the common eigenstate of T_3 and Y with eigenvalues

$$T_3 |\mu\rangle = \frac{p}{2} |\mu\rangle, \quad Y |\mu\rangle = \frac{p+2q}{3} |\mu\rangle, \quad (4)$$

and it is annihilated by $S_{01}|\mu\rangle = S_{12}|\mu\rangle = S_{02}|\mu\rangle = 0$. Analogously to the spin number $0 \leq J \leq n/2$ used to label $SU(2)$ irreps, we use here the pair of non-negative integers (p, q) to label $SU(3)$ irreps. The dimension of one such representation is then $(1+p)(1+q)(2+p+q)/2$.

$SU(3)$ Hamiltonians, such as the one describing paradigmatic spin-1 models [18], have been investigated extensively in the context of quantum chaos [32]. This is often associated to a chaotic dynamics in the classical limit, namely when taking the dimension of the irreducible representation to infinity [38, 39]. A commonly used indicator of quantum chaos consists in analyzing the nearest-neighbour energy level spacing distribution (NNSD) of the unfolded energy spectrum [32, 33]. If the NNSD follows a Poisson distribution, then the NNSD illustrates so-called ‘‘level attraction’’, that in general signals an integrable system in the classical limit. If, on the contrary, the NNSD follows a Wigner-Dyson distribution, then the NNSD illustrates so-called ‘‘level repulsion’’, which signals a chaotic system in the classical limit (equivalently described by random matrix theory). For this reason, it is convenient to fit the NNSD computed numerically with the so-called Brody distribution [40, 41], which gives a function interpolating between these two limit cases. For random matrices sampled from the Gaussian orthogonal ensemble, the Brody distribution reads

$$P(s, \omega) = A(\omega + 1)s^\omega \exp(-As^{\omega+1}), \quad (5)$$

where $A = \Gamma^{\omega+1} \left(\frac{\omega+2}{\omega+1} \right)$ and $0 \leq \omega \leq 1$ is the Brody parameter characterizing the interpolation between Poisson ($\omega \sim 0$) and Wigner-Dyson ($\omega \sim 1$) distributions. See Fig. 1 for an example.

PIBI irreducible representations and energy spacing distribution.— The PIBI Eq. (1) we have introduced is capable of detecting nonlocality in low energy states of $SU(3)$ Hamiltonians [42] that are relevant in the context of quantum chaos [18, 39, 43]. In particular, every Bell operator can itself be interpreted as an Hamiltonian whose low-energy states can show nonlocal correlations [3, 44]. This allows us to explore a possible connection between the detection of Bell nonlocality and quantum chaos. For this investigation, we proceed in the following way. First, given PIBI (1) and a number

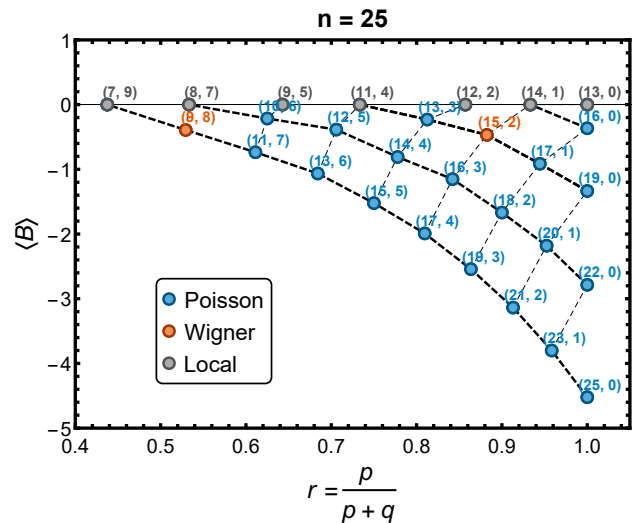


FIG. 2. Maximal quantum violation of PIBI (1) when restricted to the (p, q) irrep of $SU(3)$ for $n = 25$. The classical bound is $\beta_c = 0$ and, consequently, $\langle B \rangle < 0$ certifies nonlocality. We use $r = p/(p+q)$ as a means to quantify permutational invariance of each irrep, with $r = 1$ being the fully symmetric case. The pairs (p, q) in blue correspond to Poisson NNSD statistics (signalled by $\omega \sim 0$, integrable), while the pairs in red correspond to Wigner-Dyson NNSD statistics (signalled by $\omega > 0$, chaotic). Dashed lines connect points with same $p+q$ and $p-q$. We observe the largest amount of violation for the totally symmetric sector, as expected from PI of the Bell operator [3, 37].

of parties n , we choose an irrep (p, q) . Next, we express in this $SU(3)$ sector the Bell operator associated to our PIBI and maximize its quantum violation by optimizing over the measurement settings as explained above. Finally, we compute the NNSD of the resulting Bell operator and fit it to the Brody distribution Eq. (5) to extract the parameter ω , see e.g. Fig. 1. Repeating this approach for all inequivalent irreps (p, q) gives us a relation between quantum violations and Brody parameters ω . These results are summarized in Fig. 2 for $n = 25$, where we represent the quantum violations as a function of $r = p/(p+q) \in [0, 1]$. This parameter r can be understood as a quantifier for the degree of symmetry of each irrep, with $r = 1$ representing the fully symmetric case. Interestingly, different values of r can be associated to different classical limits where chaos may or may not manifest [39], a feature which is absent in the $SU(2)$ case. In Fig. 2 we indicate whether the NNSD associated to the specific irrep is characteristic of an integrable (blue, $\omega \sim 0$) or chaotic (orange, $\omega > 10^{-3}$) system.

From our analysis we note that, when restricting to the optimal measurements, irreps that exhibit nonlocality generically display a Poisson NNSD distribution. Conversely, irreps where no detection of nonlocality is observed generically display a Wigner-Dyson NNSD distribution. We observe this behaviour for different number of parties n , starting from $n = 8$ (when the PIBI starts detecting nonlocality) up to $n = 32$ (beyond which a numerical analysis becomes computationally expensive). Based on this observation we conjecture that,

for the PIBI Eq. (1) with optimal measurements, irreps (p, q) exhibiting nonlocality have a NNSD with $\omega \sim 0$ as n goes to infinity, which signals integrability in the classical limit. Figure 2 shows cases of irreps apparently contradicting this conjecture (the orange points below zero). However, we attribute them to finite size effects, since for $n = 25$ the scarce number of energy levels results in coarse-grained NNSDs.

Remarkably, we note the emergence of interesting patterns when plotting the maximal quantum violation for each irrep as a function of r . As an example, we highlight with thick dashed lines in Fig. 2 the connection between points with same $p+2q$, meaning a constant value of the hypercharge Y Eq. (4). The emergent structure suggests that there may be analytical expressions relating the maximal quantum violation of the PIBI with the degree of permutation symmetry in the specific subsector being probed. Exploring this potential connection is however beyond current scopes and is left for future work.

Let us emphasize that the results presented in this section are based on optimizing the measurement settings entering the PIBI. The measurement choice plays a crucial role, since it defines the Bell operator and, therefore, its quantum violation and NNSD. After having observed that when restricting to the measurements leading to maximal violation we generically obtain a Bell operator with Poisson NNSD, we proceed with exploring what happens for more general measurement choices.

Random measurement settings.— To investigate the generic case, we study here the connection between the violation of PIBI Eq. (1) and the NNSD in the case of pairs of random measurement settings. For every irrep, we have generated more than 10^3 random projectors obtained by appropriately sampling matrices from $SU(3)$ and then computed the NNSD of the resulting Bell operator. We show in Fig. 3 the histogram of the fitted Brody parameters for the illustrative case $(p, q) = (25, 0)$ and 10^4 samples.

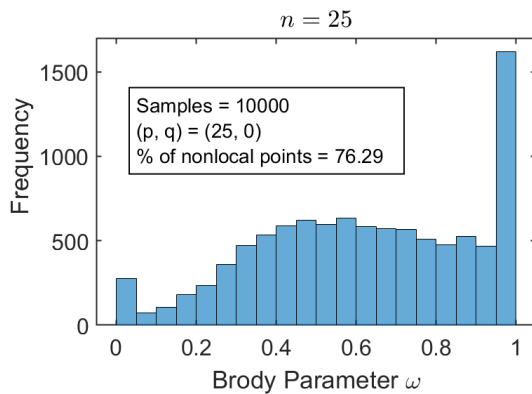


FIG. 3. Histogram of Brody parameters ω resulting from fitting the NNSD of the Bell operator constructed from the PIBI (1) using random projectors. Here $n = 25$ and $(p, q) = (25, 0)$, *i.e.* the lowest point in Fig. 2, but other irreps show a similar behaviour despite having a lower fraction of points exhibiting nonlocality.

Generically, we observe that the NNSD now approaches a

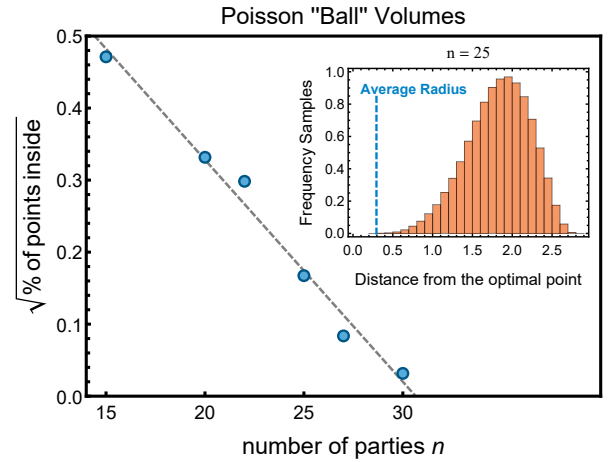


FIG. 4. Estimated volume of the region of measurement settings resulting in a Poisson NNSD plotted as a function of the number of parties n . We observe that the volume decreases as the number of parties n increases. The inset for $n = 25$ shows that only a small percentage of the randomly generated observables fall inside the estimated Poissonian region (see the text for details).

Wigner-Dyson distribution, independently of the quantum violation. Interestingly, however, note that when sampling over random projectors we obtain a high percentage of nonlocality detection. We attribute this behaviour to the restriction of using the same measurement settings for all parties. In an even more general scenario, where each party would be free to set different random measurements, we would expect the departure from Poisson NNSDs to be even more accentuated. We thus conclude that generically observing a Poisson NNSD when setting the optimal measurements for each irrep is a remarkable property, since we see that typically the Bell observable displays level-repulsion.

Volume of Poisson-like behavior around the optimal point.— To quantify the robustness of the connection between Poisson NNSD and measurement optimality, we proceed as follows. For a given n and irrep, we start from the Bell operator corresponding to the optimal measurements and then gradually deviate from it by smoothly perturbing the measurements until the NNSD of the new Bell operator stops being Poissonian. This allows us to estimate a region of measurements leading to Poisson NNSD, whose volume we observe shrinking as n increases.

For this analysis, we use the parametrization Eq. (3) to generate a random direction $\theta^{\text{rand}} \in \mathbb{R}^9$ with $\|\theta^{\text{rand}}\| \ll 1$, that we iteratively add to the optimal measurements θ^{opt} as a perturbation. At each step, we check the new Bell operator and its NNSD. After a sufficient number of iterations $\alpha \in \mathbb{N}$, we observe the NNSD transition from being Poisson ($\omega \sim 0$) to Wigner-Dyson ($\omega > 0$). The point at which this transition occurs defines the measurement settings $\tilde{\theta} = \theta^{\text{opt}} + \alpha\theta^{\text{rand}}$. By repeating this procedure for several random directions θ_j^{rand} we obtain a set of points in the measurement settings space, centered around the optimal setting,

which samples the boundary of the region where the NNSD remains Poissonian. After having collected enough boundary points $\tilde{\theta}$, we use the corresponding projectors to obtain observables $A(\tilde{\theta})$ and use the Frobenius distance to compute the average radius R^{avg} of the region with respect to the optimal settings. That is, we compute $R^{\text{avg}} = \sum_{j=1}^s R_j/s$, where s is the number of estimated boundary points we obtained and $R_j = \text{Tr} \left[\left(A(\theta^{\text{opt}}) - A(\tilde{\theta}_j) \right) \left(A(\theta^{\text{opt}}) - A(\tilde{\theta}_j) \right)^\dagger \right]^{1/2}$. Therefore, we identify R^{avg} as the radius of a ball approximating the Poissonian region. Finally, we use a Monte Carlo method to estimate the volume of this region: we generate random observables $A(\theta)$ and estimate their membership in the Poissonian region. Concretely, we check whether their radius R is smaller or larger than the average radius of the region R^{avg} . To ensure that the random observables have been generated uniformly, we construct them from random unitaries $U \in \mathbb{C}^{3 \times 3}$ sampled from the Haar measure.

In Fig. 4, for each shown value of n we have estimated the Poissonian regions using 10^3 random directions and 10^5 random unitaries U . We observe that the volumes associated to Poisson NNSD become smaller as the number of parties increases. Our numerical study suggests that this volume tends to zero in the asymptotic limit. Therefore, this further supports our conjecture that the Poisson NNSD observed around the point maximally violating the Bell inequality (1) is indeed a special case. This observation applies to the maximal violation of each irrep displaying nonlocality.

Conclusions and outlook.— We have investigated the connection between Bell nonlocality and quantum chaos. To this end, we introduced a novel two-input three-outcome multipartite Bell inequality and computed for qutrits the Bell operators resulting from different choices of measurement settings. We have characterized the NNSD of these operators and found that, generically, measurements yielding maximal violation give Poisson statistics, while non-optimal measurements give Wigner-Dyson statistics.

Our results lead us to conjecture that, in the thermodynamic limit, only the optimal measurement settings lead to a Bell operator with NNSD characteristic of an integrable system. Even a slight perturbation from these settings, although it would not alter the amount of Bell violation observed, quickly results in an operator characteristic of a chaotic system.

Our work represents a first step towards using Bell inequalities as a diagnostic tool to probe quantum chaos. The structure present in the points of maximal violation suggest that the absence of chaos can allow for elegant characterizations of the quantum state and measurements, which is an essential ingredient for self-testing of quantum many-body systems [45]. In future works, it would be interesting to further explore how our findings manifest in more general Bell scenarios.

Acknowledgments.— AA acknowledges support from the Austrian Science Fund (FWF) (projects P 33730-N and 10.55776/PAT2839723) and by the ESQ Discovery programme (Erwin Schrödinger Center for Quantum Science &

Technology), hosted by the Austrian Academy of Sciences (ÖAW).

GM and ML acknowledge support from: European Research Council AdG NOQIA; MCIN/AEI (PGC2018-0910.13039/501100011033, CEX2019-000910-S/10.13039/501100011033, Plan National FIDEUA PID2019-106901GB-I00, Plan National STAMEENA PID2022-139099NB, I00, project funded by MCIN/AEI/10.13039/501100011033 and by the “European Union NextGenerationEU/PRTR” (PRTR-C17.I1), FPI); QUANTERA MAQS PCI2019-111828-2); QUANTERA DYNAMITE PCI2022-132919, QuantERA II Programme co-funded by European Union’s Horizon 2020 program under Grant Agreement No 101017733); Ministry for Digital Transformation and of Civil Service of the Spanish Government through the QUANTUM ENIA project call - Quantum Spain project, and by the European Union through the Recovery, Transformation and Resilience Plan - NextGenerationEU within the framework of the Digital Spain 2026 Agenda; Fundació Cellex; Fundació Mir-Puig; Generalitat de Catalunya (European Social Fund FEDER and CERCA program, AGAUR Grant No. 2021 SGR 01452, Quantum-CAT U16-011424, co-funded by ERDF Operational Program of Catalonia 2014-2020); Barcelona Supercomputing Center MareNostrum (FI-2023-3-0024); Funded by the European Union. Views and opinions expressed are however those of the author(s) only and do not necessarily reflect those of the European Union, European Commission, European Climate, Infrastructure and Environment Executive Agency (CINEA), or any other granting authority. Neither the European Union nor any granting authority can be held responsible for them (HORIZON-CL4-2022-QUANTUM-02-SGA PASQuanS2.1, 101113690, EU Horizon 2020 FET-OPEN OPTologic, Grant No 899794), EU Horizon Europe Program (This project has received funding from the European Union’s Horizon Europe research and innovation program under grant agreement No 101080086 NeQSTGrant Agreement 101080086 — NeQST); ICFO Internal “QuantumGaudi” project; European Union’s Horizon 2020 program under the Marie Skłodowska-Curie grant agreement No 847648; “La Caixa” Junior Leaders fellowships, La Caixa” Foundation (ID 100010434): CF/BQ/PR23/11980043.

JT has received support from the European Union’s Horizon Europe program through the ERC StG FINE-TEA-SQUAD (Grant No. 101040729). JT also acknowledges support from the Quantum Delta NL program. This publication is part of the ‘Quantum Inspire – the Dutch Quantum Computer in the Cloud’ project (with project number [NWA.1292.19.194]) of the NWA research program ‘Research on Routes by Consortia (ORC)’, which is funded by the Netherlands Organization for Scientific Research (NWO).

MF was supported by the Swiss National Science Foundation Ambizione Grant No. 208886, and The Branco Weiss Fellowship – Society in Science, administered by the ETH Zürich.

* albert.aloy@oeaw.ac.at

† fadelm@phys.ethz.ch

- [1] N. Brunner, D. Cavalcanti, S. Pironio, V. Scarani, and S. Wehner, *Rev. Mod. Phys.* **86**, 419 (2014).
- [2] I. Frérot, M. Fadel, and M. Lewenstein, *Reports on Progress in Physics* **86**, 114001 (2023).
- [3] M. Fadel and J. Tura, *Quantum* **2**, 107 (2018).
- [4] A. Piga, A. Aloy, M. Lewenstein, and I. Frérot, *Physical Review Letters* **123** (2019).
- [5] F. Fröwis, M. Fadel, P. Treutlein, N. Gisin, and N. Brunner, *Phys. Rev. A* **99**, 040101 (2019).
- [6] D. Alsina, A. Cervera, D. Goyeneche, J. I. Latorre, and K. Życzkowski, *Phys. Rev. A* **94**, 032102 (2016).
- [7] G. Müller-Rigat, A. Aloy, M. Lewenstein, and I. Frérot, *PRX Quantum* **2**, 030329 (2021).
- [8] B. Chazelle, *Discrete & Computational Geometry* **10**, 377 (1993).
- [9] J. Tura, A. B. Sainz, T. Vértesi, A. Acín, M. Lewenstein, and R. Augusiak, *Journal of Physics A: Mathematical and Theoretical* **47**, 424024 (2014).
- [10] Z. Wang, S. Singh, and M. Navascués, *Phys. Rev. Lett.* **118**, 230401 (2017).
- [11] J. Tura, R. Augusiak, A. B. Sainz, T. Vértesi, M. Lewenstein, and A. Acín, *Science* **344**, 1256 (2014).
- [12] S. Wagner, R. Schmied, M. Fadel, P. Treutlein, N. Sangouard, and J.-D. Bancal, *Physical Review Letters* **119**, 170403 (2017).
- [13] F. Baccari, J. Tura, M. Fadel, A. Aloy, J.-D. Bancal, N. Sangouard, M. Lewenstein, A. Acín, and R. Augusiak, *Physical Review A* **100** (2019).
- [14] M. Fadel and J. Tura, *Phys. Rev. Lett.* **119**, 230402 (2017).
- [15] J. Guo, J. Tura, Q. He, and M. Fadel, *Phys. Rev. Lett.* **131**, 070201 (2023).
- [16] R. Schmied, J.-D. Bancal, B. Allard, M. Fadel, V. Scarani, P. Treutlein, and N. Sangouard, *Science* **352**, 441 (2016).
- [17] N. J. Engelsen, R. Krishnakumar, O. Hosten, and M. A. Kasevich, *Phys. Rev. Lett.* **118**, 140401 (2017).
- [18] H. Lipkin, N. Meshkov, and A. Glick, *Nuclear Physics* **62**, 188 (1965).
- [19] N. Meshkov, A. Glick, and H. Lipkin, *Nuclear Physics* **62**, 199 (1965).
- [20] A. Glick, H. Lipkin, and N. Meshkov, *Nuclear Physics* **62**, 211 (1965).
- [21] C. K. Law, H. Pu, and N. P. Bigelow, *Phys. Rev. Lett.* **81**, 5257 (1998).
- [22] C. D. Hamley, C. S. Gerving, T. M. Hoang, E. M. Bookjans, and M. S. Chapman, *Nature Physics* **8**, 305 (2012).
- [23] J. Kitzinger, X. Meng, M. Fadel, V. Ivannikov, K. Nemoto, W. J. Munro, and T. Byrnes, *Phys. Rev. A* **104**, 043323 (2021).
- [24] X.-Y. Luo, Y.-Q. Zou, L.-N. Wu, Q. Liu, M.-F. Han, M. K. Tey, and L. You, *Science* **355**, 620 (2017).
- [25] F. D. M. Haldane, *Physics Letters A* **93**, 464 (1983).
- [26] F. D. M. Haldane, *Phys. Rev. Lett.* **50**, 1153 (1983).
- [27] I. Affleck, T. Kennedy, E. H. Lieb, and H. Tasaki, *Phys. Rev. Lett.* **59**, 799 (1987).
- [28] S. Fishman, D. R. Grempel, and R. E. Prange, *Phys. Rev. Lett.* **49**, 509 (1982).
- [29] F. Haake, M. Kuś, and R. Scharf, *Zeitschrift für Physik B Condensed Matter* **65**, 381 (1987).
- [30] O. Bohigas, M. J. Giannoni, and C. Schmit, *Phys. Rev. Lett.* **52**, 1 (1984).
- [31] M. L. Mehta, *Random matrices* (Elsevier, 2004).
- [32] F. Haake, S. Gnutzmann, and M. Kuś, *Quantum Signatures of Chaos* (Springer International Publishing, 2018).
- [33] See supplementary materials.
- [34] A. Aloy, M. Fadel, and J. Tura, *New Journal of Physics* **23**, 033026 (2021).
- [35] A. Vourdas, *Reports on Progress in Physics* **67**, 267 (2004).
- [36] J. Kaniewski, I. Šupić, J. Tura, F. Baccari, A. Salavrakos, and R. Augusiak, *Quantum* **3**, 198 (2019).
- [37] J. Tura, R. Augusiak, A. Sainz, B. Lücke, C. Klempt, M. Lewenstein, and A. Acín, *Annals of Physics* **362**, 370 (2015).
- [38] L. G. Yaffe, *Rev. Mod. Phys.* **54**, 407 (1982).
- [39] S. Gnutzmann, F. Haake, and M. Kus, *Journal of Physics A: Mathematical and General* **33**, 143 (1999).
- [40] T. A. Brody, *Lettere al Nuovo Cimento (1971-1985)* **7**, 482 (1973).
- [41] E. Bittner, H. Markum, and R. Pullirsch, (2001), [arXiv:hep-lat/0110222 \[hep-lat\]](https://arxiv.org/abs/hep-lat/0110222).
- [42] G. Müller-Rigat, A. Aloy, M. Lewenstein, M. Fadel, and J. Tura, “Three-outcome multipartite bell inequalities: applications to dimension witnessing and spin-nematic squeezing in many-body systems,” [arXiv today](https://arxiv.org/abs/2303.10000).
- [43] D. C. Meredith, S. E. Koonin, and M. R. Zirnbauer, *Physical Review A* **37**, 3499 (1988).
- [44] J. Tura, G. De las Cuevas, R. Augusiak, M. Lewenstein, A. Acín, and J. I. Cirac, *Phys. Rev. X* **7**, 021005 (2017).
- [45] I. Šupić and J. Bowles, *Quantum* **4**, 337 (2020).
- [46] R. Shurtleff, “Formulas for $su(3)$ matrices,” (2023), [arXiv:0908.3864 \[math-ph\]](https://arxiv.org/abs/0908.3864).

SUPPLEMENTAL MATERIAL FOR “BELL INEQUALITIES AS A TOOL TO PROBE QUANTUM CHAOS”

Classical bound for the Bell inequality (1)

Here we provide a proof showing that the Bell inequality B introduced in the main text has classical bound $\beta_c = 0$ for any number of parties n . That is, we want to show that

$$B = (\mathcal{P}_{0|0} + \mathcal{P}_{0|1} + \mathcal{P}_{1|0} + \mathcal{P}_{1|1}) + (\mathcal{P}_{00|00} + \mathcal{P}_{00|11} + \mathcal{P}_{11|00} + \mathcal{P}_{11|11}) - 2(\mathcal{P}_{01|01} + \mathcal{P}_{01|10}) \geq 0. \quad (6)$$

First, in order to account for all local hidden variables, we want to come up with a parametrization to describe the conditional probabilities in terms of Local Deterministic Strategies (LDS). Because our Bell inequality is permutationally invariant, many Bell inequality coefficients take the same values at many LDSs, which leads to redundancies. Hence, instead of considering all the d^{mn} possibilities of the general case (3^{2n} for our case with 3 outcomes and 2 measurements), we propose the following (much more efficient) parametrization: Suppose that at each run all the outcomes for each possible measurement and party are predetermined. Then, let $c_{a,a'}$ be the total number of parties that have predetermined the pair of outcomes $a, a' \in \{0, 1, 2\}$ for the two possible measurement settings $x \in \{0, 1\}$ respectively. It follows by definition that $c_{a,a'} \geq 0$ and $\sum_{a,a'} c_{a,a'} = n$. Therefore, following this parametrization, the symmetrized one-body conditional probabilities $\mathcal{P}_{a|x}$ under a given LDS can be expressed as:

$$\mathcal{P}_{a|x} := \sum_{i=1}^n p_i(a|x) \stackrel{\text{LDS}}{=} \begin{cases} c_{a,0} + c_{a,1} + c_{a,2} & \text{for } x = 0 \\ c_{0,a} + c_{1,a} + c_{2,a} & \text{for } x = 1 \end{cases}. \quad (7)$$

On the other hand, the symmetric two-body conditional probabilities $\mathcal{P}_{ab|xy}$ factorize under a given LDS as:

$$\begin{aligned} \mathcal{P}_{ab|xy} &:= \sum_{i \neq j} p_{ij}(ab|xy) \stackrel{\text{LDS}}{=} \sum_{i \neq j} p_i(a|x)p_j(b|y) \\ &= \underbrace{\sum_{i \neq j} p_i(a|x)p_j(b|y)}_{\mathcal{P}_{a|x}\mathcal{P}_{b|y}} + \underbrace{\sum_i p_i(a|x)p_i(b|y)}_{:=Q_{ab|xy}} - \sum_i p_i(a|x)p_i(b|y), \end{aligned} \quad (8)$$

where we have defined

$$Q_{ab,xy} := \begin{cases} \mathcal{P}_{a|x} & \text{if } a = b, x = y \\ 0 & \text{if } a \neq b, x = y \\ c_{a,b} & \text{if } x = 0, y = 1 \\ c_{b,a} & \text{if } x = 1, y = 0 \end{cases}. \quad (9)$$

Note that one can neglect one of the outcomes without loss of generality by means of the NS principle,

$$P(a_1, \dots, \hat{a}_i, \dots, a_n | x_1, \dots, \hat{x}_i, \dots, x_n) \equiv \sum_{a_i \in \{0,1,2\}} P(a_1, \dots, a_n | x_1, \dots, x_n),$$

where $\hat{\cdot}$ denotes the absence of that coordinate and the \equiv symbol means that the LHS of Eq. (10) is well-defined; *i.e.*, it does not depend on the value of x_i . Hence, for instance we can take Eqs. (7) to (9) with $a, b \in \{0, 1\}$. Notice also that it is straightforward to generalize our parametrization to any number of outcomes d .

Finally, in Tab. I we express the one-body terms and the factorized two-body terms as a function of the quantities $c_{a,a'}$. Therefore, all the possible local-realist correlations in a $(n, 2, 3)$ Bell-type experiments can be described in terms of the relations in Table I and shared randomness. Moreover, the local polytope for an $(n, 2, 3)$ permutationally invariant Bell scenario characterized by one- and two-body correlators is formed by the convex hull of all the configurations satisfying the relations in Table I.

$$\begin{array}{cccccc} \mathcal{P}_{0|0} \stackrel{\text{LDS}}{=} c_{0,0} + c_{0,1} + c_{0,2} & \mathcal{P}_{00|00} \stackrel{\text{LDS}}{=} \mathcal{P}_{0|0}^2 - \mathcal{P}_{0|0} & \mathcal{P}_{00|01} \stackrel{\text{LDS}}{=} \mathcal{P}_{0|0}\mathcal{P}_{0|1} - c_{0,0} & \mathcal{P}_{00|10} \stackrel{\text{LDS}}{=} \mathcal{P}_{00|01} & \mathcal{P}_{00|11} \stackrel{\text{LDS}}{=} \mathcal{P}_{0|1}^2 - \mathcal{P}_{0|1} \\ \mathcal{P}_{1|0} \stackrel{\text{LDS}}{=} c_{1,0} + c_{1,1} + c_{1,2} & \mathcal{P}_{01|00} \stackrel{\text{LDS}}{=} \mathcal{P}_{0|0}\mathcal{P}_{1|0} & \mathcal{P}_{01|01} \stackrel{\text{LDS}}{=} \mathcal{P}_{0|0}\mathcal{P}_{1|1} - c_{0,1} & \mathcal{P}_{01|10} \stackrel{\text{LDS}}{=} \mathcal{P}_{10|01} & \mathcal{P}_{01|11} \stackrel{\text{LDS}}{=} \mathcal{P}_{0|1}\mathcal{P}_{1|1} \\ \mathcal{P}_{0|1} \stackrel{\text{LDS}}{=} c_{0,0} + c_{1,0} + c_{2,0} & \mathcal{P}_{10|00} \stackrel{\text{LDS}}{=} \mathcal{P}_{0|100} & \mathcal{P}_{10|01} \stackrel{\text{LDS}}{=} \mathcal{P}_{1|0}\mathcal{P}_{0|1} - c_{1,0} & \mathcal{P}_{10|10} \stackrel{\text{LDS}}{=} \mathcal{P}_{01|01} & \mathcal{P}_{10|11} \stackrel{\text{LDS}}{=} \mathcal{P}_{01|11} \\ \mathcal{P}_{1|1} \stackrel{\text{LDS}}{=} c_{0,1} + c_{1,1} + c_{2,1} & \mathcal{P}_{11|00} \stackrel{\text{LDS}}{=} \mathcal{P}_{1|100}^2 - \mathcal{P}_{1|10} & \mathcal{P}_{11|01} \stackrel{\text{LDS}}{=} \mathcal{P}_{1|0}\mathcal{P}_{1|1} - c_{1,1} & \mathcal{P}_{11|10} \stackrel{\text{LDS}}{=} \mathcal{P}_{11|01} & \mathcal{P}_{11|11} \stackrel{\text{LDS}}{=} \mathcal{P}_{1|1}^2 - \mathcal{P}_{1|1} \end{array}$$

TABLE I. Resulting one- and two-body conditional probabilities under an LDS.

Now that we have a parametrization to incorporate the LDSs into the conditional probabilities, we are ready to substitute the corresponding conditional probabilities in the Bell inequality. After rearranging the terms, one ends up with the following polynomial:

$$\begin{aligned} B = & (c_{00} + c_{02})^2 + (c_{00} + c_{20})^2 + (c_{11} + c_{12})^2 + (c_{11} + c_{21})^2 \\ & + (c_{00} - c_{12})^2 + (c_{00} - c_{21})^2 + (c_{11} - c_{02})^2 + (c_{11} - c_{20})^2 \\ & + 2(c_{10} + c_{01}) - 2(c_{00} + c_{11})^2 - (c_{12} + c_{20})^2 - (c_{02} + c_{21})^2, \end{aligned} \quad (10)$$

where $c_{i,j} \geq 0$ for all $i, j \in \{0, 1, 2\}$ and they fulfill the constraint $\sum_{0 \leq i, j < 3} c_{ij} = n$ with n the total number of parties. Notice that the term c_{22} does not appear in the expression, thus we can set any $0 \leq c_{22} \leq n$ without contributing in the classical bound. Thus it is trivial to see that there exists at least one strategy leading to $B = 0$, i.e. setting $c_{22} = n$. Consequently, we just have to prove that B cannot take negative values.

Proof that $B \geq 0$: We are interested in the minimal value that (10) can achieve. Since the terms $2(c_{10} + c_{01})$ will always add a positive or zero contribution, we can set them to $c_{10} = c_{01} = 0$ without loss of generality to find the minimal value of B . Therefore we simplify the problem to look at the minimal value of:

$$\begin{aligned} \tilde{B} = & (c_{00} + c_{02})^2 + (c_{00} + c_{20})^2 + (c_{11} + c_{12})^2 + (c_{11} + c_{21})^2 \\ & + (c_{00} - c_{12})^2 + (c_{00} - c_{21})^2 + (c_{11} - c_{02})^2 + (c_{11} - c_{20})^2 \\ & - 2(c_{00} + c_{11})^2 - (c_{12} + c_{20})^2 - (c_{02} + c_{21})^2. \end{aligned} \quad (11)$$

After expanding and rearranging the terms we reach the following equivalent polynomial:

$$\begin{aligned} \tilde{B} = & 2 \left[c_{00}^2 + c_{11}^2 + \frac{c_{02}^2 + c_{20}^2}{2} + \frac{c_{12}^2 + c_{21}^2}{2} \right. \\ & + c_{00}(c_{02} + c_{20}) - c_{11}(c_{02} + c_{20}) + c_{11}(c_{12} + c_{21}) - c_{00}(c_{12} + c_{21}) \\ & \left. - c_{02}c_{21} - c_{12}c_{20} - 2c_{00}c_{11} \right]. \end{aligned} \quad (12)$$

Then, the condition for (12) to take negative values corresponds to the following inequality

$$c_{11}(c_{02} + c_{20}) + c_{00}(c_{12} + c_{21}) + c_{02}c_{21} + c_{12}c_{20} + 2c_{00}c_{11} > c_{00}^2 + c_{11}^2 + \frac{c_{02}^2 + c_{20}^2}{2} + \frac{c_{12}^2 + c_{21}^2}{2} + c_{00}(c_{02} + c_{20}) + c_{11}(c_{12} + c_{21}), \quad (13)$$

which can be rearranged as:

$$(c_{00} - c_{11})(c_{12} + c_{21} - c_{02} - c_{20}) > (c_{00} - c_{11})^2 + \frac{(c_{02} - c_{21})^2}{2} + \frac{(c_{12} - c_{20})^2}{2}. \quad (14)$$

Our goal is to find that such condition leads to a contradiction for all cases in order to show that I cannot take a negative value. First it is convenient to define the variables $x := c_{00} - c_{11}$, $y := c_{12} - c_{20}$, $z := c_{02} - c_{21}$, so that the condition gets expressed as:

$$x(y - z) - \left(x^2 + \frac{y^2}{2} + \frac{z^2}{2} \right) > 0. \quad (15)$$

Take now $f(x, y, z) = x(y - z) - \left(x^2 + \frac{y^2}{2} + \frac{z^2}{2} \right)$ in order to find its critical points $\nabla f(x, y, z) = (-2x + y - z, x - y, -z - x)$, $\nabla f(x^*, y^*, z^*) = 0 \Rightarrow x^* = y^*, z^* = -x^*$, where $f(x^*, y^*, z^*) = 0$. Next, by looking at its Hessian matrix $\mathbf{H}(f(x, y, z))$, where $(\mathbf{H}(f(x, y, z)))_{ij} = \frac{\partial^2 f}{\partial x_i \partial x_j}$, one sees that the resulting Hessian matrix has eigenvalues $\{-3, -1, 0\}$ and therefore it is negative semidefinite. Thus, the critical point corresponds to the maximum.

We conclude that (15) leads to a contradiction for all values of c_{ij} and, consequently, I cannot take negative values. Finally, since the argument is independent of n and we have seen that $I = 0$ is a valid local deterministic strategy, it follows that the classical bound is $\beta_c = 0$ for all n .

Measurement optimization restricted to some irreducible representation of SU(3)

In the task of optimizing the measurement settings for a specific irrep, one encounters the problem of representing the symmetrized version of a one-body observable A in that specific irrep. Normally, general formulas for an irrep (p, q) exist only for specific matrices, so one has to do the appropriate change of coordinates to represent an arbitrary A in the irrep (p, q) . Here we outline this method. Following the notation of Ref. [46], we start by fixing the eight basis matrices with the identity element $\{\mathbb{I}, T_+, T_-, T^3, V_+, V_-, U_+, U_-, U^3\}^{(p,q)}$ of the finite dimensional (p, q) -irrep of SU(3). In Ref. [46] one can find a possible representation of these for any (p, q) . Then, define G as the Gram matrix formed from this basis for the local irrep $(p, q) = (1, 0)$; i.e., $G_{i,j} = \langle v_i, v_j \rangle$, for $v_i \in \{\mathbb{I}, T_+, T_-, T^3, V_+, V_-, U_+, U_-, U^3\}^{(1,0)}$. Next, define a column-vector $\mathbf{b} = (\langle v_1, A \rangle, \langle v_2, A \rangle, \dots, \langle v_9, A \rangle)^T$ consisting of the inner products of this basis for some one-party observable A parametrized as described in the text. Finally, solve the system of linear equations $G\mathbf{x} = \mathbf{b}$ in order to find \mathbf{x} . We are now ready to represent an observable A in any chosen irrep (p, q) through the following expression

$$A^{(p,q)} = nx_1\mathbb{I}^{(p,q)} + \sum_{i=2}^9 x_i v_i^{(p,q)}, \quad (16)$$

where the first term has been taken out of the sum to go together with the extra identity elements that need to be added in order to guarantee the proper normalization.

Now, if we choose the one-party observable A to be a one-body projective unitary qudit operator (for example, $A = \mathcal{P}_{0|0}$), we can use the approach introduced in the main text, which allows us to perform typical optimization techniques restricted to the chosen irrep (p, q) subsector. Finally, the two-body terms take the form

$$\mathcal{P}_{ab|xy}^{(p,q)} = \mathcal{P}_{ax}^{(p,q)} \mathcal{P}_{by}^{(p,q)} - (\mathcal{P}_{ax} \mathcal{P}_{by})^{(p,q)}. \quad (17)$$

Unfolding the energy spectrum

To compare the nearest neighbour energy level space distribution of different operators, it is desirable to normalize it appropriately. The procedure we follow takes the name of spectrum unfolding [32] and it consists of the following steps.

First, the energy spectrum is sorted so that the energy levels $\{x_i\}_i$ are in ascending order $\{x_1 \leq x_2 \leq \dots \leq x_k\}$. Then, we compute the cumulative distribution function $I_x(E)$ counting the number of energy levels up to energy E . This is a discrete function, which it is convenient to interpolate with a continuous polynomial function $\tilde{I}_x(E)$. The goal is now to rescale the sequence $\{x_i\}_i$ into a sequence $\{y_i\}_i$, such that its cumulative function $\tilde{I}_y(E)$ is a straight line. This is achieved by inverting the function $\tilde{I}_x(E)$ and using it to rescale the sequence $\{x_i\}_i$. This spectrum unfolding ensures that the local density of states of the renormalized levels $\{y_i\}_i$ is unity. From the latter sequence we compute the nearest-neighbour energy level spacing as $s_i = y_i - y_{i-1}$, which are used to obtain the NNSD.
